

Hybrid Integrated Dual-Microcomb Source

Nikita Yu. Dmitriev^{1,2,*}, Sergey N. Koptyaev^{3,†}, Andrey S. Voloshin^{4,‡}, Nikita M. Kondratiev^{1,‡}, Kirill N. Min'kov¹, Valery E. Lobanov^{1,‡}, Maxim V. Ryabko³, Stanislav V. Polonsky³, and Igor A. Bilenko^{1,5,†}


¹*Russian Quantum Center, Skolkovo 143026, Russia*

²*Moscow Institute of Physics and Technology (MIPT), Dolgoprudny, Moscow Region 141701, Russia*

³*Samsung R&D Institute Russia, SAIT-Russia Laboratory, Moscow 127018, Russia*

⁴*Institute of Physics, Swiss Federal Institute of Technology Lausanne (EPFL), Lausanne CH-1015, Switzerland*

⁵*Faculty of Physics, Lomonosov Moscow State University, Moscow 119991, Russia*

 (Received 7 April 2022; revised 27 June 2022; accepted 15 July 2022; published 26 September 2022)

Dual-comb interferometry is based on self-heterodyning two optical frequency combs, with corresponding mapping of the optical spectrum into the radio-frequency domain. The dual comb enables diverse applications, including metrology, fast high-precision spectroscopy with high signal-to-noise ratio, distance ranging, and coherent optical communications. However, current dual-frequency-comb systems are designed for research applications and typically rely on scientific equipment and bulky mode-locked lasers. Here we demonstrate a fully integrated power-efficient dual-microcomb source that is electrically driven and allows turnkey operation. Our implementation uses commercially available components, including distributed-feedback and Fabry-Perot laser diodes, and silicon-nitride photonic circuits with microresonators fabricated in commercial multiproject wafer runs. Our devices are therefore unique in terms of size, weight, power consumption, and cost. Laser-diode self-injection locking relaxes the requirements on microresonator spectral purity and Q factor, so that we can generate soliton microcombs resilient to thermal frequency drift and with pump-to-comb sideband efficiency of up to 40% at mW power levels. We demonstrate down-conversion of the optical spectrum from 1400 to 1700 nm into the radio-frequency domain, which is valuable for fast wide-band Fourier spectroscopy, which was previously not available with chip-scale devices. Our findings pave the way for further integration of miniature microcomb-based sensors and devices for high-volume applications, thus opening up the prospect of innovative products that redefine the market of industrial and consumer mobile and wearable devices and sensors.

DOI: [10.1103/PhysRevApplied.18.034068](https://doi.org/10.1103/PhysRevApplied.18.034068)

I. INTRODUCTION

Over the past few decades, optical frequency combs have become a versatile tool for addressing scientific and technical challenges [1–3]. One of the most promising and widely employed applications is the use of a double (or dual) optical comb for the efficient transfer of signals from the optical domain into the rf range, thus greatly simplifying data acquisition and subsequent processing. For instance, dual-comb spectroscopy is a remarkable form of Fourier spectroscopy, enabling ultrafast measurement of broadband optical absorption spectra that provide fingerprints of specific materials or their quantity in the sample using a single photodetector, without the need for moving components, and only a few basic optical

components [4–9]. The basic idea of the dual-comb technique is to combine two coherent optical frequency combs with shifted pump lines (f_1, f_2) and slightly different line spacing in the frequency domain ($f_{\text{rep}1}, f_{\text{rep}2}$) [Fig. 1(a)]. Thereby, the optical spectrum of the combs transmitted through the matter is down-converted at the photodetector into the rf band for measurement. The resulting signal is a rf frequency comb with $\delta = |f_{\text{rep}1} - f_{\text{rep}2}|$ line spacing, a central line located at $\Delta = |f_1 - f_2|$, and line amplitudes uniquely defined by the corresponding lines of the optical combs. These characteristics make dual-comb techniques highly attractive for myriad practical applications, such as ultrabroadband near-IR spectroscopy [10,11], near-field microscopy for subwavelength spatial resolution [12,13], precision metrology of molecular-line center frequencies [14], greenhouse-gas monitoring [15–17], combustion diagnosis [18], and distance ranging (LIDAR) [19–23].

There exist a number of rapidly developing approaches for implementing dual-comb techniques. Various dual-comb systems are based on conventional fiber mode-locked

*nkdmiriev@gmail.com

†igorbilenko@gmail.com

‡These authors contributed equally to this work.

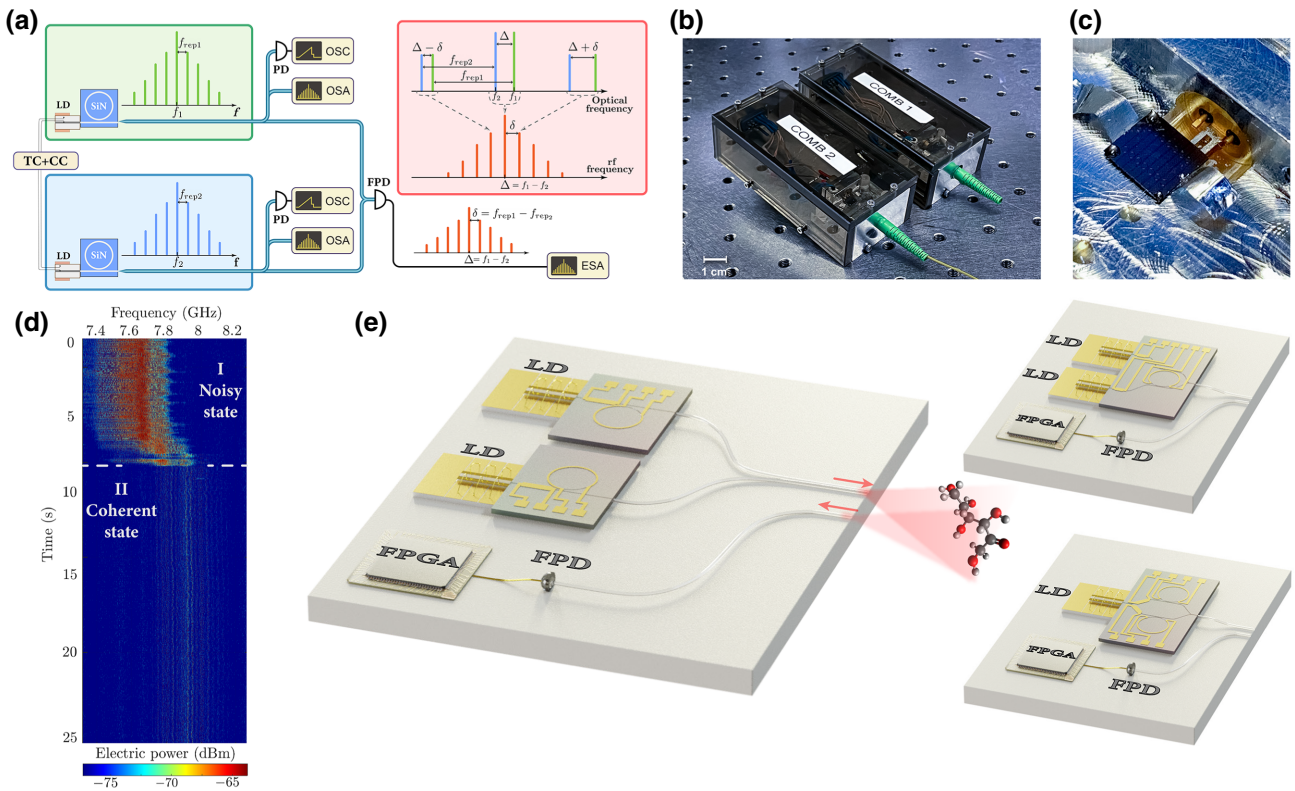


FIG. 1. Principle of the hybrid integrated dual-microcomb source. (a) Sketch of the experimental setup illustrating integrated dual-comb signal generation based on the two separate soliton microcomb sources (marked with green and blue rectangles): LD, semiconductor laser diode; SiN, photonic chip with high- Q silicon nitride microresonator; TC and CC, temperature and current controllers; FPD, fast photodetector; OSA, optical spectrum analyzer; ESA, electrical spectrum analyzer. (b) Photograph of the portable turnkey dual-comb source comprising two standalone matched integrated soliton microcomb sources. (c) Interior view of the assembled microcomb source: the glued photonic chip butt coupled to the laser diode and the output lensed fiber. (d) Evolution of the experimentally observed dual-comb signal based on two matched soliton microcombs during the search for the operating point. Demonstration of the dual-comb signal transition from a noisy (area I) to a soliton state (area II) by fine tuning the LD current. (e) Various concepts of dual-comb spectrometers: two separate microcomb-generating photonic chips pumped with two LDs; single photonic chip generating two microcombs pumped with two LDs; and single photonic chip generating two microcombs pumped with a single LD. FPGA is a field-programmable gate array.

lasers (MLLs) [24–27]. The use of mode-locked integrated external-cavity surface-emitting lasers (MIXSELS) potentially allows dual-comb signal generation with a single cavity, exploiting different polarization states [28,29]. Hybrid THz dual-comb spectrometers based on quantum cascade lasers (QCLs) [30] and coherently averaged dual-comb spectrometers [31] demonstrated fast and high-accuracy spectroscopy measurements in the mid-wavelength infrared (MWIR) and long-wavelength infrared (LWIR) ranges. These results have been obtained in laboratory settings, which means that many of these dual-comb systems are only partially integrated and rather bulky and complicated, requiring a range of auxiliary equipment and technical expertise. As a consequence, they are not suitable for industrial and consumer applications, despite outstanding performance in laboratory environments. Therefore, integration and device miniaturization are pressing issues that need to be addressed before any of

the approaches can be utilized in industrial-grade devices. Fully integrated dual-comb systems hold the promise to unlock major applications, including airborne and spaceborne sensors, distance ranging with unprecedented speed and resolution, and compact spectroscopy sensors. In turn, such devices could become a core technology for consumer and wearable applications, including noninvasive spectroscopic sensors.

The most promising platform for a fully integrated dual-comb source is silicon-based integrated photonics. In recent years, this platform has experienced major advances and reached considerable maturity [32–34]. Today, the performance of low-loss silicon-based photonic systems has become comparable with that of free-space optic systems. In addition, high-level compatibility with CMOS fabrication processes [35–37] and also with the III-V semiconductor platform [38–40] have been demonstrated. Recent progress in silicon photonics, combined with the

self-injection locking (SIL) effect [41–49], enabled optical microcomb generation using semiconductor laser diodes (LDs) instead of bulky narrow-linewidth lasers, thereby greatly simplifying the process of microcomb generation and paving the way for the development of fully integrated chip-scale single microcomb sources based on high- Q microresonators (MRs) [38,39,50–52]. Proof-of-concept experiments based on passive high- Q MRs achieved broadband optical spectrum down-conversion to the rf range, generating ultrawide frequency combs with widely variable (from GHz to THz) line spacing in the near-infrared (NIR), SWIR, and visible-wavelength ranges in bulk and on-chip structures [53–63]. Also, the recently demonstrated scanning dual-comb spectroscopy (SDCS) technique allows additionally the resolution of spectroscopic systems to be increased based on high- Q MRs [58].

Here, we report a feasibility study of dual-comb integration and introduce the hybrid integrated dual-microcomb source for the SWIR range based on commercially available low-cost components [Figs. 1(b) and 1(c)]. With the assembled prototype we successfully down-convert a 300-nm-wide optical spectrum to a 600-MHz-wide rf signal. Our findings establish that electrically driven soliton microcombs comprising integrated SiN high- Q MRs combined with SIL semiconductor LDs [Fig. 1(a)] are a promising technology platform for highly integrated energy-efficient dual-comb sources covering wide spectral ranges. Specifically, we demonstrate that SIL provides up to 40% pump-to-comb sideband conversion efficiency (η_{p2c}) for bright solitons. In the light of such a high conversion value we consider in detail the η_{p2c} efficiency of SIL-enabled generation of bright dissipative Kerr solitons in photonic chip-based microresonators, and its dependence on key parameters. In this way we find that SIL relaxes the requirements on MR properties such as Q factor, spectral purity, the number of mode crossings, the width of a so-called “soliton step,” making it possible to generate microcombs with the majority of commercial photonic chip-based MRs featuring moderate Q factors. SIL greatly facilitates tuning to the soliton regime, due to the compensation of the thermal effects inevitable in systems where a free-running laser is used as a pump source. Consequently, SIL enables soliton microcomb generation in cases where it is otherwise not possible with optically isolated external-cavity diode lasers (ECDLs).

The here-presented prototype of the integrated dual-microcomb source, based on laser diode self-injection locked to a microresonator, combined all the benefits of Fourier-transform infrared broadband spectroscopy in a chip-scale spectroscopic sensor and looks promising as a platform for future mobile and wearable devices. The demonstrated versatile approach to dual-microcomb source integration provides various design options [Fig. 1(e)], offering interesting perspectives in terms of device miniaturization and performance, in

particular, with a view to broadband infrared dual-comb sensors for high-volume applications. With further integration, there is a clear route to satisfying the so-called SWaP-C (size, weight, power and cost) requirements that are extremely important for industrial, airborne, space, and consumer applications.

II. RESULTS

A. Hybrid integrated platform for optical dual-microcomb source

Our hybrid integrated dual-microcomb source comprises specially matched (see Methods and Note S1 within the Supplemental Material [64]) microcomb sources. Each consists of a thermally stabilized SiN photonic chip with a high- Q MR, a butt-coupled semiconductor LD, and an output lensed fiber [Fig. 1(a)–1(c)]. This versatile approach enables fast prototyping by testing different photonic chip designs and various types of LDs.

The MRs based on CMOS-compatible SiN photonic chips that we use in our experiments are fabricated in commercial multiproject wafer (MPW) runs. We use two sets of chips with MRs of two diameters, corresponding to approximately 150 GHz and to approximately 1-THz free spectral range (FSR) with integrated microheaters enabling grid matching of the eigenfrequencies of different MRs by tuning their FSR (spacing between fundamental modes in the frequency domain) [65,66]. Also, each chip has edge waveguide couplers, ensuring insertion losses as low as -1.1 dB on both sides of a chip for coupling light in and out.

Fabry-Perot (FP) and distributed feedback (DFB) laser diodes are used for experiments and are compared in terms of performance for microcomb generation (see Methods and Note S2 within the Supplemental Material [64]). FP diodes have a single spatial mode, 35-GHz longitudinal mode spacing, 1535-nm central wavelength, and approximately 200-mW optical power at 500 mA of injection current. DFB diodes have 1545-nm wavelength and optical power of approximately 100 mW at 400 mA.

During the experiment we simultaneously monitor the optical spectra of the microcombs and the resulting rf dual-comb signal using an optical spectrum analyzer (OSA) and an electrical spectrum analyzer (ESA). Owing to the SIL effect, the assembled microcomb sources offer reproducible turnkey operation, allowing generation of the microcomb with the same envelope for fixed setup time after time. This kind of turnkey operation was described in Ref. [50] and also demonstrated in Ref. [67]. The spectrogram presented in Fig. 1(d) shows dual-comb signal evolution while selecting the turnkey operating point by slow manual tuning of the LD injection current. Away from the operating point, the optical spectrum consists of one coherent soliton microcomb and one chaotic noncoherent microcomb (MI state). The heterodyne

beatnote signal of this state is noisy [regime I in Fig. 1(d)]. When the LD-current value reaches the operating point, the system locks to the state with both soliton microcombs, featuring high mutual coherence and low-noise rf beatnotes of the optical components [regime II in Fig. 1(d)]. The SIL mechanism compensates thermal effects and the microcomb sources lock to the comb states without additional manipulations, which are inevitable when pumping with a free-running laser. At the operating point, our dual-microcomb source quickly transits to a coherent state. However, it should be noted that due to the independent thermal stabilization of the two photonic chips, a relative thermal drift of the rf beat frequencies, up to 100 MHz, arises for observation periods exceeding several minutes. Nevertheless, there is no change of the rf microcomb envelope in time, since the detuning is fixed due to the SIL.

B. Highly efficient soliton microcombs for dual-microcomb source

Current technology used in the fabrication of high- Q silicon nitride MRs, especially for commercially available runs, does not guarantee Q factors higher than one million and a spectral purity of MRs sufficient high for sustainable soliton microcomb generation using external pumping with single-frequency narrow-linewidth lasers.

The procedure of soliton comb excitation by means of an external pump using ECDL requires accessible soliton steps and is complicated by the need for additional equipment to achieve a high tuning rate and to overcome thermal instabilities [68]. We note that in our experiments only high-FSR MRs ($\text{FSR} = 1$ THz) provide easily accessible soliton steps and support soliton generation using ECDL.

We are not able to observe soliton generation with 150-GHz MRs using the external amplified ECDL providing more than 150 mW of in-chip pump power. This power level is more than 10 times higher than the parametric instability threshold, corresponding to the normalized pump amplitude $f = \sqrt{P_{\text{pump}}/P_{\text{th}}} > 3$, where P_{pump} is the optical power of the amplified ECDL reduced by losses for the butt coupling of the lensed fiber with the chip (power in the bus waveguide) and P_{th} is the nonlinearity threshold power [68]. Apparently, the influence of thermal processes, high-order dispersion [Fig. 3(a)] and avoided mode-crossing points shortens a soliton step and makes it inaccessible [see Fig. 2(b)] [69–74].

However, the fully integrated SIL scheme [Fig. 2(c)] provides outstanding turnkey operation without any additional equipment. The same MR pumped by the self-injection locked LD allows clear observation of a soliton step in the locked state, even for $f \sim 1.6$ [Fig. 2(d) and 2(e)]. Indeed, most of the thermal effects are

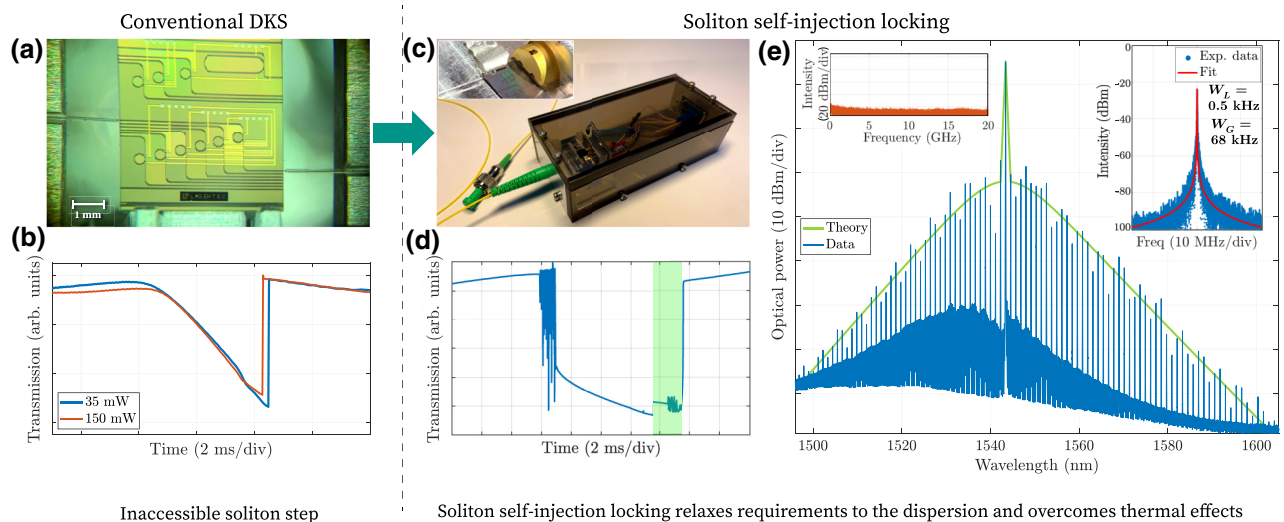


FIG. 2. Soliton microcomb generation using self-injection-locked laser-diode pumping in the case of an inaccessible conventional soliton step. (a) Photograph of the silicon nitride photonic chip used in the experiment. (b) Nonlinear-resonance shape for the different pump powers of the external optically isolated laser, demonstrating inaccessibility of the conventional soliton step. The measured nonlinear threshold of this microresonator is approximately 13 mW. (c) Photograph of the assembled prototype of the microcomb source, based on the same photonic chip pumped with a butt-coupled Fabry-Perot laser diode. Inset: inside view the prototype. (d) Nonlinear-resonance shape for 35-mW pump power for the same resonance shown in (b) for the case of the self-injection locking effect (laser-diode pumping). The area where the soliton exists is highlighted in green color. (e) Output of the microcomb source (blue line) and theoretically predicted envelope of the single soliton state microcomb spectrum (green line) based on the measured microresonator parameters (see Note S4 within the Supplemental Material [64]). Left inset: rf spectrum of the output signal. Right inset: beatnote signal of the generated microcomb line and a Toptica CTL-1550 tunable laser recorded with a resolution bandwidth (RBW) of 10 kHz (blue points), together with a Voigt-profile fit (red line) with 0.5- and 68-kHz Lorentzian and Gaussian widths, respectively.

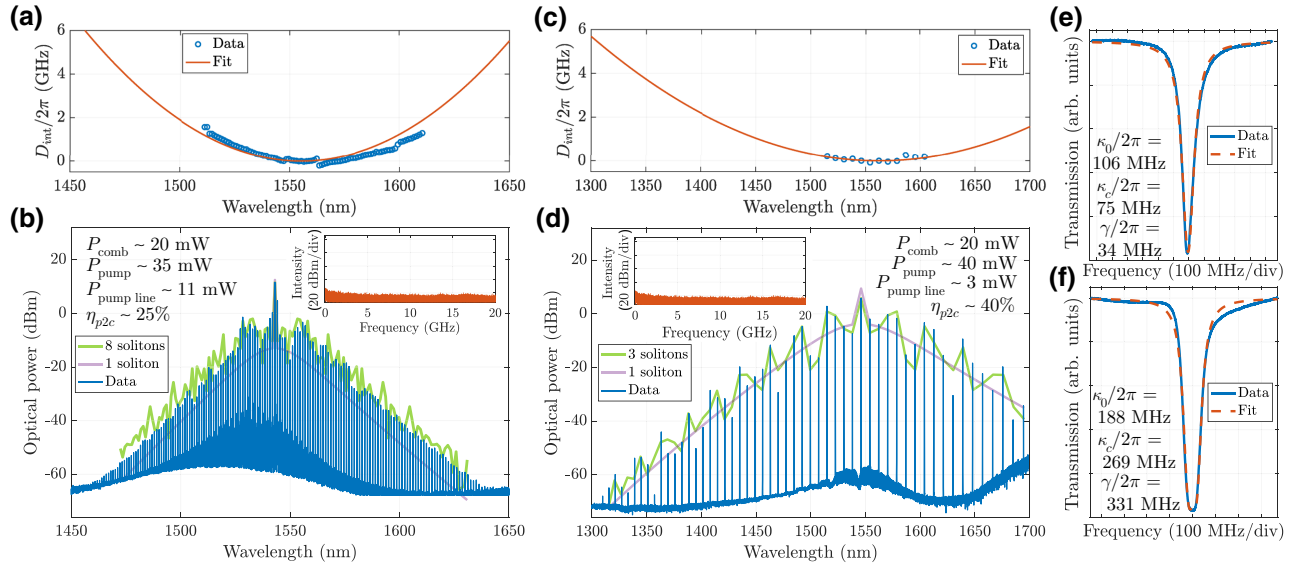


FIG. 3. High-power and broadband microcombs in 150-GHz and 1-THz microresonators. (a),(c) Measured and fitted anomalous dispersion landscape in a Si_3N_4 microresonator with $\text{FSR} = 143.6$ and 999.8 GHz, and estimated second-order dispersion coefficient $D_2/2\pi \approx 1.38$ and ≈ 14.3 MHz, respectively. (b),(d) Optical spectra of generated high-power microcomb with approximately 150 GHz (b) and approximately 1 THz (d) repetition rate (blue lines) and values of key parameters: total comb power (P_{comb}), laser diode power (P_{pump}), the power of the microcomb central line (pump line) ($P_{\text{pump line}}$), and pump-to-comb sideband conversion efficiency (η_{p2c}). Theoretically predicted envelope for corresponding microcombs based on measured microresonator parameters (see Note S4 within the Supplemental Material [64]) for single-soliton state (green line) and multisoliton state (purple line). (e),(f) Experimentally measured resonances in the linear regime (blue line) and loaded Lorentzian profile fits (red dashed line) for approximately 150 GHz (e) and approximately 1 THz (f) microresonators. The estimated intrinsic loss (κ_0), coupling rate (κ_c), and backward-wave coupling rate (γ) correspond to a coupling coefficient $\eta = 0.42$ and 0.59 , and Q factor approximately 1.8×10^6 and approximately 1×10^6 for 150-GHz and 1-THz microresonators, respectively.

suppressed as the laser frequency is locked to the MR and the laser-microresonator detuning ζ_{eff} is fixed. If the MR frequency fluctuates due to the thermal effects, the generation frequency also changes, keeping the comb-generation regime stable [75]. In the SIL regime the laser-microresonator detuning becomes fixed to the value $\zeta_{\text{eff}}^0 \approx -3(f^2/2)^{1/3} + (f^2/2)^{-1/3}$ (for small backscattering and $f > 1$), which lies inside the soliton-generation region $\zeta_{\text{eff}} \in [-\pi^2 f^2/8; -3(f^2/4)^{1/3} + (f^2/4)^{-1/3}/4]$ [76–78] (see Note S3 within the Supplemental Material [64]).

In addition, the detuning control is much more robust in the SIL regime as the effective detuning does not change while the LD is tuned within the locking range. More precisely, the speed of the laser-frequency tuning is effectively reduced by the factor of the stabilization coefficient K_0 (see Note S3 within the Supplemental Material [64]).

The assembled prototype works as a turnkey device, and thereby greatly simplifies the process of comb generation and significantly improves its stability. Once calibrated to define the operating point, this device can generate microcombs immediately after being turned on.

Microcomb spectra and the microresonator parameters are shown in Fig. 3. Notably, there are no optical elements filtering the pump line. Despite the moderate Q factor (approximately 10^6), the generated combs are broadband.

The spectrum width of the microcombs with 1-THz line spacing reaches 500 nm, with 20 lines of power > -20 dBm. The width of the 150-GHz microcomb spectrum exceeds 200 nm, with 30 lines of power > -20 dBm. The generated microcombs also feature high optical power per line and therefore a high signal-to-noise ratio, and demonstrates high pump-to-comb sideband power conversion efficiency (η_{p2c}). The latter can be expressed as $\eta_{p2c} = (P_{\text{comb}} - P_{\text{pump line}})/P_{\text{pump}}$, where P_{comb} is the total generated microcomb power in the output fiber, $P_{\text{pump line}}$ is the power of the microcomb central line (pump line) in the output fiber, and P_{pump} is the optical power of the free-running laser diode for the same injection current value reduced by the coupling losses (power in the bus waveguide). For the 150-GHz microcomb, $P_{\text{comb}} \approx 20$ mW, $P_{\text{pump line}} \approx 11$ mW, and $P_{\text{pump}} \approx 35$ mW; for the 1-THz microcomb, $P_{\text{comb}} \approx 20$ mW, $P_{\text{pump line}} \approx 3$ mW, and $P_{\text{pump}} \approx 40$ mW. Evaluated η_{p2c} efficiency values for the 150-GHz and 1-THz FSR microcombs are 25% and 40%, respectively. Before this work, comparable efficiency has been demonstrated for the generation of dark microcombs only [79,80]. The high efficiencies obtained are in a good agreement with our estimates (see Note S4 within the Supplemental Material [64]) and are compatible with Ref. [81,82].

C. Spectral characteristics of dual-microcomb source

Combined microcomb optical spectra and the resulting rf dual-microcomb signals are shown in Figs. 4(a), 4(d), 4(g) and in Figs. 4(b), 4(c), 4(e), 4(f), 4(h), 4(i), respectively. Insets in the bottom row give information about the linewidth of the lines of the generated dual-microcomb signal, estimated with Voigt-profile fits (W_L is the Lorentzian linewidth and W_G the Gaussian linewidth). With 1-THz FSR microresonators we successfully down-convert approximately 300-nm-wide optical spectra to 600-MHz-wide spectra in the rf range [Figs. 4(a)–4(f)]; with 150-GHz FSR microresonators we achieve down-conversion from approximately 100 nm to 800 MHz [Figs. 4(g)–4(i)].

By applying voltage to the microheaters we can adjust the microresonator temperature and thereby control the

microcomb line spacing. One optical microcomb can be shifted relatively to the other to control the dual-microcomb signal, changing its central line position Δ and repetition rate δ . This capability is illustrated in Figs. 4(a)–4(f). These two dual-microcomb signals are observed for the same pair of MRs, and using microheaters we change the central-frequency difference Δ from 7.93 to 1.70 GHz.

Verification of the measurement data is conducted by comparing the experimental data with the theoretically predicted beatnote signal of the two combined optical microcombs. Knowing the MR parameters, including dispersion profile, and with the measured optical frequency combs, we can calculate the expected dual-comb spectrum profile in the rf domain. These simulated dual-microcomb spectra are shown as gray lines in Figs. 4(c), 4(f), 4(i).

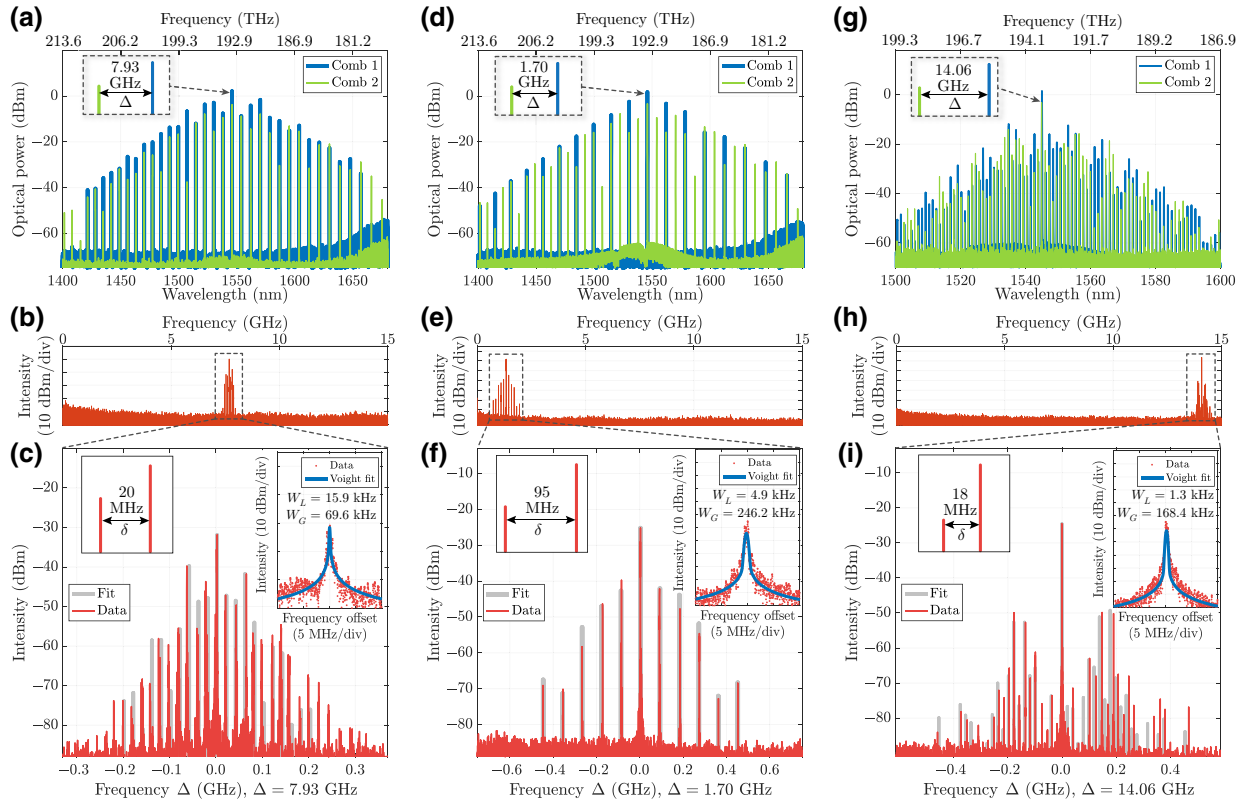


FIG. 4. Dual-microcomb signals. Top row: optical spectra of the generated microcombs that are combined for dual-microcomb signal generation. Inset: enlargement of the central line area, with the distance between them (Δ) indicated. Bottom row: the dual-microcomb signal is a rf comb with central line at Δ and repetition rate $\delta = |f_{\text{rep}1} - f_{\text{rep}2}|$, where $f_{\text{rep}1}$ are the repetition rates of the combined optical combs. The top full-span spectrum (from 0 to 15 GHz) demonstrates the absence of low-frequency noise, showing a strong dual-microcomb signal. The bottom spectrum is an enlargement of the central (frequency, Δ) dual-microcomb signal area. The red line is the experimentally observed signal and the gray line the predicted signal based on the optical spectra above. Inset: estimation of the rf-comb linewidth from a Voigt-profile fit. (a),(b),(c) Dual-comb signal obtained by combining two optical frequency combs with $f_{\text{rep}1} \sim f_{\text{rep}2} \sim 1$ THz and $\delta = |f_{\text{rep}1} - f_{\text{rep}2}| \approx 20$ MHz. The distance between the pump lines of the optical microcombs is $\Delta = 7.93$ GHz. (d),(e),(f) Dual-microcomb signal obtained by combining two optical frequency combs with repetition rates $f_{\text{rep}1} \sim 1$ THz, $f_{\text{rep}2} \sim 2$ THz, and $\delta = |2f_{\text{rep}1} - f_{\text{rep}2}| \approx 95$ MHz. The distance between the pump lines of the optical microcombs is $\Delta = 1.70$ GHz. (g),(h),(i) Dual-microcomb signal obtained by combining two optical frequency combs with $f_{\text{rep}1} \sim f_{\text{rep}2} \sim 150$ GHz and $\delta = |f_{\text{rep}1} - f_{\text{rep}2}| \approx 18$ MHz. The distance between the pump lines of the optical microcombs is $\Delta = 14.06$ GHz.

III. DISCUSSION

We find that SIL relaxes the requirements on the microresonator Q factor and its spectral purity, and makes widely available microresonators commercially fabricated in MPW run suitably for use in on-chip dual-microcomb sources. Note that soliton-comb excitation with such microresonators pumped by a tunable optically isolated ECDL (not SIL) is unsuccessful, because the required soliton steps could not be accessed [Fig. 2(b)]. We connect this failure with the influence of the thermal processes, high-order dispersion effects, and avoided mode-crossing points, which makes the soliton step shorter and therefore inaccessible. In case of the SIL effect, the frequencies of the laser diode and the microresonator are connected and fluctuate in a correlated manner, resulting in microcomb generation with higher tolerance to thermal drift [Fig. 2(d)].

The demonstrated pump-to-comb sideband conversion efficiency of up to 40% can be explained by the matching between Q factor and pump power, taking into account the following considerations. First, the comb power does not depend directly on the pump power (see Note S4 within the Supplemental Material [64]). Although both the maximal and the locked detunings do depend on the pump power, these dependencies are weaker, and the pump-to-soliton (and pump-to-comb sideband) power conversion efficiency decreases with it. This creates the illusion that using a low-power laser and reducing the threshold we can make a highly energy-efficient device. However, the second point is that the comb power does depend on the threshold power of the parametric instability. Therefore, using the strategy described above, we end up with a negligible output signal. This brings us to the rather counterintuitive conclusion that for best performance, the threshold power should be increased (meaning lower Q factors or less nonlinearity, for example) and matched with the used laser pump power. This immediately brings up a trade-off problem, as the lower Q factor means less stabilization and wider beatnote or even the self-injection locking regime cannot be reached at all. Another way to increase the pump-to-comb sideband power conversion efficiency is increasing the second-order dispersion coefficient. This presents, however, a trade-off problem for the comb width, which should be solved separately for the desired application.

We also can see an additional mechanism to increase the comb power (and subsequently the power efficiency). In our system, multisoliton states can emerge; however, the number of solitons has a maximum for a given dispersion value [83] and the pump-to-comb sideband conversion efficiency (η_{p2c}) also saturates with it (see Note S4 within the Supplemental Material [64]). The multisoliton option is realized for the 1-THz microresonator [see Fig. 3(d)], where we find good correspondence of the measured spectrum with the theoretical prediction for three-soliton states

(the soliton positions are optimized to fit the data) for the experimentally estimated parameters (f , D_2 , κ) and SIL detuning value (ζ_{eff}^0). We note that while the form of the spectrum is highly dependent on the intersoliton distances, the total comb power (and the conversion efficiency) does not. For the 150-GHz comb we see a slightly different picture. By increasing the number of solitons we are able to match the total comb output power, but the comb envelope at the sides show much smoother behavior than the multisoliton state can provide [see green curve in Fig. 3(b)]. At the same time, the comb power is too high for a single-soliton state [see purple curve in Fig. 3(d)]. Such a comb enhancement can be attributed to the comb-line amplification inside the active medium of the laser or so-far unexplored effects of the multifrequency locking, while the nonsmooth envelope near the pump—to the dispersion distortions from the mode crossings [70].

A comparison of the semiconductor FP and DFB laser diodes highlights the benefits of DFB in terms of predictable wavelength of locking and more convenient matching of two combs, while the FP is much more powerful and cheaper, and hence more promising with a view to practical applications.

The early integrated dual-microcomb source prototype presented here is still affected by the relative thermal drift of the microresonators on the two separate photonic chips. The amplitude of the thermal drift does not exceed 100 MHz and the typical time is about 2–3 min. Various design options [Fig. 1(e)] could help to overcome the drift, paving the way to more compact devices. A first improvement could be the combination of the two microresonators on the same photonic chip positioned on a common temperature-stabilized substrate with two pumping laser diodes. This option would simplify comb matching owing to small fabrication errors for the two microresonators at close distance, thus enhancing the stability of the dual-comb beatnotes. The next improvement for higher stability and smaller size is using the same microresonator for the generation of two soliton combs propagating in the same or opposite directions along the ring, similarly as it was demonstrated in Ref. [84] for optically isolated lasers. Two laser diodes self-injection locked into the same microresonator provide the highest mutual coherence [85] and generated microcombs would lead to dual-comb beatnotes with the lowest phase noise. To reduce the number of components that need to be aligned during the integration, keeping small size and high stability, the design option with just one laser diode and one photonic chip with two microresonator could be considered. A laser diode locked to one of the microresonators would provide the first microcomb and the second resonator tuned relative to the frequency of the locked laser would provide the second one. The discussed design options based on the microcomb generation using self-injection locking should improve the performance of the integrated dual-microcomb source, and

will be explored in future research. Though the obvious evolution of the dual combs are single-chip devices, the presented approach has obvious advantages as it allows thermal cross-talk to be avoided, simplifying packaging and tuning.

Taking into account recent advances of III-V heterogeneous integration with silicon-nitride photonic waveguides [38], deeper integration of the proposed dual-microcomb source can lead to reaching tiny chip-scale sizes. Also, the demonstrated possibility to use FP laser diodes might allow using just a gain section without an additional laser cavity in future generations of the chip-based dual-comb sources.

In conclusion, obtained results demonstrate that SIL Kerr microcombs based on silicon photonics can successfully compete with other on-chip optical-comb sources and outperform them owing to the unique combination of power efficiency with mWs comb power, a wider spectrum, and low phase noise.

ACKNOWLEDGMENTS

This work is supported by the Russian Science Foundation (Grant No. 20-12-00344). V.E.L. and N.Yu.D. acknowledge personal support from the Foundation for the Advancement of Theoretical Physics and Mathematics “BASIS.” A.S.V. is supported by the EU H2020 research and innovation programme under the Marie Skłodowska-Curie Grant Agreement No. 101033663 (RaMSoM). N.Yu.D. is partially supported by the Samsung Research Center in Moscow. The authors thank H.-S. Lee and Y.-G. Roh from the Samsung Advanced Institute of Technologies for help in establishing the project and its further support. Authors express special thanks to Alexander Gorodnitskiy, graduate student of MIPT and Sofya Agafonova, student of MIPT for assistance at an early stage of experiments.

COMPETING INTERESTS

S.N.K., A.S.V., V.E.L., M.V.R., S.V.P., and I.A.B. are listed as co-authors in joint Samsung Electronics and Russian Quantum Center US Patent No. US10224688B2, which is related to the technology reported in this paper. The authors declare no competing interests.

APPENDIX A: SILICON-NITRIDE-CHIP CHARACTERISATION

The SiN photonic chip-based microresonators used in our experiments are fabricated by Ligentec SA, Switzerland. The pumped microresonator resonance is measured using an external tunable laser Toptica CTL1550, and fitted taking backscattering into account [86] to obtain the intrinsic loss κ_0 , the coupling rate κ_c , and the backward-wave coupling rate γ (mode splitting). Based on these data,

we evaluate the full resonance linewidth $\kappa = \kappa_0 + \kappa_c$, the pump coupling efficiency $\eta = \kappa_c/\kappa$, and the normalized backscattering coefficient $\beta = \gamma/\kappa$.

For nonlinearity-threshold estimation the experimental setup with the external laser Toptica CTL1550 and a booster NKT Photonics Koheras Boostik HP E15 is used. Gradually increasing the pump power, we simultaneously monitor the optical spectrum and the resonance shape using an OSA (Yokogawa AQ6370D) and an oscilloscope (Keysight DSO-X 3024A). First, we reach the thermal nonlinearity threshold ($P_{\text{th}}^{\text{Thermal}}$), where the resonance shape becomes triangular. By further increasing the pump power, we reach the parametric instability threshold (P_{th}), accompanied by sideband generation.

Dispersion characteristics of microresonators are measured using the original experimental setup based on the tunable laser Toptica CTL1550 and a calibrated fiber Mach-Zehnder interferometer (MZI) with a FSR of 102 MHz.

The results obtained for the 150-GHz and 1-THz FSR microresonators, respectively, are as follows: $\kappa_0/2\pi = 106$ and 188 MHz, $\kappa_c/2\pi = 75$ and 269 MHz, $\gamma/2\pi = 34$ and 331 MHz, $\eta = 0.42$ and 0.59, Q factor = 1.8×10^6 and 1×10^6 , $P_{\text{th}} = 14$ and 11 mW, $P_{\text{th}}^{\text{Thermal}} = 3.7$ and 2.5 mW, $D_1/2\pi = 143.6$ and 999.8 GHz, and $D_2/2\pi = 1.38$ and 14.3 MHz.

APPENDIX B: MICROCOMB SOURCE

After chip characterization we successfully generate microcombs with all available chips and compare the reproducibility of their parameters (see Note S1 within the Supplemental Material [64]). As a result, we match photonic chips for rf dual-microcomb signal generation and define the operating points for all laser diodes and photonic chip pairs, which are used for the assembly process. The operating point is defined by the following parameters: laser-diode temperature, injection current, and microheater voltage.

In addition, we compare two types of laser diodes, DFB and FP (Seminox, USA), in terms of their suitability for being used for microcomb generation (see Note S2 within the Supplemental Material [64]).

We also estimate the linewidth of the microcomb components using the heterodyne technique. The beatnote signal between the external laser and the microcomb line is presented in the inset of Figs. 3(e), 3(f). The Lorentzian width of the beatnote signal (estimated using a Voigt-profile fit) is 0.5 kHz. The Gaussian width is about 68 kHz, which can be improved by further reduction of the technical noises.

[1] Th. Udem, R. Holzwarth, and T. W. Hänsch, Optical frequency metrology, *Nature* **416**, 233 (2002).

- [2] Tara Fortier and Esther Baumann, 20 years of developments in optical frequency comb technology and applications, *Commun. Phys.* **2**, 153 (2019).
- [3] Scott A. Diddams, Kerry Vahala, and Thomas Udem, Optical frequency combs: Coherently uniting the electromagnetic spectrum, *Science* **369**, eaay3676 (2020).
- [4] Myoung-Gyun Suh, Qi-Fan Yang, Ki Youl Yang, Xu Yi, and Kerry J. Vahala, Microresonator soliton dual-comb spectroscopy, *Science* **354**, 600 (2016).
- [5] Ian Coddington, Nathan Newbury, and William Swann, Dual-comb spectroscopy, *Optica* **3**, 414 (2016).
- [6] Takuro Ideguchi, Dual-comb spectroscopy, *Opt. Photon. News* **28**, 32 (2017).
- [7] Nathalie Picqué and Theodor W. Hänsch, Frequency comb spectroscopy, *Nat. Photonics* **13**, 146 (2019).
- [8] Esther Baumann, Eli V. Hoenig, Edgar F. Perez, Gabriel M. Colacion, Fabrizio R. Giorgetta, Kevin C. Cossel, Gabriel Ycas, David R. Carlson, Daniel D. Hickstein, Kartik Srinivasan, Scott B. Papp, Nathan R. Newbury, and Ian Coddington, Dual-comb spectroscopy with tailored spectral broadening in Si₃N₄ nanophotonics, *Opt. Express* **27**, 11869 (2019).
- [9] S. N. Koptyaev, G. V. Lihachev, N. G. Pavlov, A. A. Shechkin, I. A. Bilenko, M. V. Riabko, M. L. Gorodetsky, S. V. Polonsky, A. S. Voloshin, and A. D. Lantsov *et al.*, Optical dual-comb source apparatuses including optical microresonator, (2019), US Patent 10, 224, 688.
- [10] Sho Okubo, Kana Iwakuni, Hajime Inaba, Kazumoto Hosaka, Atsushi Onae, Hiroyuki Sasada, and Feng-Lei Hong, in *CLEO: 2014* (Optical Society of America, San Jose, California United States, 2014), p. STh1N.6.
- [11] Sho Okubo, Kana Iwakuni, Hajime Inaba, Kazumoto Hosaka, Atsushi Onae, Hiroyuki Sasada, and Feng-Lei Hong, Ultra-broadband dual-comb spectroscopy across 1.0–1.9 μm , *Appl. Phys. Express* **8**, 082402 (2015).
- [12] Markus Brehm, Albert Schliesser, and Fritz Keilmann, Spectroscopic near-field microscopy using frequency combs in the mid-infrared, *Opt. Express* **14**, 11222 (2006).
- [13] H.-G. von Ribbeck, M. Brehm, D. W. van der Weide, S. Winnerl, O. Drachenko, M. Helm, and F. Keilmann, Spectroscopic thz near-field microscope, *Opt. Express* **16**, 3430 (2008).
- [14] A. M. Zolot, F. R. Giorgetta, E. Baumann, W. C. Swann, I. Coddington, and N. R. Newbury, Broad-band frequency references in the near-infrared: Accurate dual comb spectroscopy of methane and acetylene, *J. Quant. Spectrosc. Radiat. Transfer* **118**, 26 (2013).
- [15] E. Baumann, F. R. Giorgetta, W. C. Swann, A. M. Zolot, I. Coddington, and N. R. Newbury, Spectroscopy of the methane ν_3 band with an accurate midinfrared coherent dual-comb spectrometer, *Phys. Rev. A* **84**, 062513 (2011).
- [16] G. B. Rieker, F. R. Giorgetta, W. C. Swann, J. Kofler, A. M. Zolot, L. C. Sinclair, E. Baumann, C. Cromer, G. Petron, C. Sweeney, P. P. Tans, I. Coddington, and N. R. Newbury, Frequency-comb-based remote sensing of greenhouse gases over kilometer air paths, *Optica* **1**, 290 (2014).
- [17] F Zhu, A Bicer, R Askar, J Bounds, A. A. Kolomenskii, V Kelessides, M Amani, and H. A. Schuessler, Mid-infrared dual frequency comb spectroscopy based on fiber lasers for the detection of methane in ambient air, *Laser Phys. Lett.* **12**, 095701 (2015).
- [18] P. J. Schroeder, R. J. Wright, S. Coburn, B. Sodergren, K. C. Cossel, S. Droste, G. W. Truong, E. Baumann, F. R. Giorgetta, I. Coddington, N. R. Newbury, and G. B. Rieker, Dual frequency comb laser absorption spectroscopy in a 16 MW gas turbine exhaust, *Proc. Combust. Inst.* **36**, 4565 (2017).
- [19] I. Coddington, W. C. Swann, L. Nenadovic, and N. R. Newbury, Rapid and precise absolute distance measurements at long range, *Nat. Photonics* **3**, 351 (2009).
- [20] Myoung-Gyun Suh and Kerry J. Vahala, Soliton micro-comb range measurement, *Science* **359**, 884 (2018).
- [21] P. Trocha, M. Karpov, D. Ganin, M. H. P. Pfeiffer, A. Kordts, S. Wolf, J. Krockenberger, P. Marin-Palomo, C. Weimann, S. Randel, W. Freude, T. J. Kippenberg, and C. Koos, Ultrafast optical ranging using microresonator soliton frequency combs, *Science* **359**, 887 (2018).
- [22] Jacob Nürnberg, Benjamin Willenberg, Christopher R. Phillips, and Ursula Keller, Dual-comb ranging with frequency combs from single cavity free-running laser oscillators, *Opt. Express* **29**, 24910 (2021).
- [23] Johann Riemensberger, Anton Lukashchuk, Maxim Karpov, Wenle Weng, Erwan Lucas, Junqiu Liu, and Tobias J. Kippenberg, Massively parallel coherent laser ranging using a soliton microcomb, *Nature* **581**, 164 (2020).
- [24] I. Coddington, W. C. Swann, and N. R. Newbury, Coherent dual-comb spectroscopy at high signal-to-noise ratio, *Phys. Rev. A* **82**, 043817 (2010).
- [25] Nazanin Hoghooghi, Ryan K. Cole, and Gregory B. Rieker, 11- μs time-resolved, continuous dual-comb spectroscopy with spectrally filtered mode-locked frequency combs, *Appl. Phys. B* **127**, 1 (2021).
- [26] M. Imrul Kayes, Nurmemet Abdukerim, Alexandre Rekik, and Martin Rochette, Free-running mode-locked laser based dual-comb spectroscopy, *Opt. Lett.* **43**, 5809 (2018).
- [27] Sandro M. Link, Alexander Klenner, and Ursula Keller, Dual-comb modelocked lasers: Semiconductor saturable absorber mirror decouples noise stabilization, *Opt. Express* **24**, 1889 (2016).
- [28] S. M. Link, C. A. Zaugg, Alexander Klenner, M. Mangold, M. Golling, B. W. Tilma, and U. Keller, in *Vertical External Cavity Surface Emitting Lasers (VECSELs) V*, (International Society for Optics and Photonics, San Francisco, California, United States, 2015), Vol. 9349, p. 93490Q.
- [29] Jacob Nürnberg, Cesare G. E. Alfieri, Dominik Waldburger, L. Krüger, Matthias Golling, and Ursula Keller, in *2019 Conference on Lasers and Electro-Optics Europe & European Quantum Electronics Conference (CLEO/Europe-EQEC)* (IEEE, Munich, Germany, 2019), p. 1.
- [30] Luigi Consolino, Malik Nafa, Michele DeRegis, Francesco Cappelli, Katia Garrasi, Francesco P. Mezzapesa, Lianhe Li, A. Giles Davies, Edmund H. Linfield, Miriam S. Vitiello, Saverio Bartalini, and Paolo De Natale, Quantum cascade laser based hybrid dual comb spectrometer, *Commun. Phys.* **3**, 69 (2020).
- [31] K. Komagata, A. Shehzad, G. Terrasanta, Pierre Brochard, R. Matthey, M. Gianella, Pierre Jouy, Filippos Kapsalidis, M. Shahmohammadi, Mattias Beck, V. J. Wittwer, J. Faist, L. Emmenegger, T. Südmeyer, A. Hugi, and S. Schilt, Coherently-averaged dual comb spectrometer at 7.7 μm with master and follower quantum cascade lasers, *Opt. Express* **29**, 19126 (2021).

- [32] Martin H. P. Pfeiffer, Arne Kordts, Victor Brasch, Michael Zervas, Michael Geiselmann, John D Jost, and Tobias J Kippenberg, Photonic Damascene process for integrated high- Q microresonator based nonlinear photonics, *Optica* **3**, 20 (2016).
- [33] Junqiu Liu, Arslan S. Raja, Maxim Karpov, Bahareh Ghadiani, Martin H. P. Pfeiffer, Botao Du, Nils J. Engelsen, Hairun Guo, Michael Zervas, and Tobias J. Kippenberg, Ultralow-power chip-based soliton microcombs for photonic integration, *Optica* **5**, 1347 (2018).
- [34] Junqiu Liu, Guan hao Huang, Rui Ning Wang, Jijun He, Arslan S. Raja, Tianyi Liu, Nils J. Engelsen, and Tobias J. Kippenberg, High-yield, wafer-scale fabrication of ultralow-loss, dispersion-engineered silicon nitride photonic circuits, *Nat. Commun.* **12**, 1 (2021).
- [35] Michael Hochberg and Tom Baehr-Jones, Towards fabless silicon photonics, *Nat. Photonics* **4**, 492- (2010).
- [36] Michael Hochberg, Nicholas C. Harris, Ran Ding, Yi Zhang, Ari Novack, Zhe Xuan, and Tom Baehr-Jones, Silicon photonics: the next fabless semiconductor industry, *IEEE Solid-State Circuits Mag.* **5**, 48 (2013).
- [37] C. Weimann, M. Lauer mann, F. Hoeller, W. Freude, and C. Koos, Silicon photonic integrated circuit for fast and precise dual-comb distance metrology, *Opt. Express* **25**, 30091 (2017).
- [38] Chao Xiang, Junqiu Liu, Joel Guo, Lin Chang, Rui Ning Wang, Wenle Weng, Jonathan Peters, Weiqiang Xie, Zeyu Zhang, Johann Riemensberger, Jennifer Selvidge, Tobias J. Kippenberg, and John E. Bowers, Laser soliton microcombs heterogeneously integrated on silicon, *Science* **373**, 99 (2021).
- [39] Chao Xiang, Joel Guo, Warren Jin, Lue Wu, Jonathan Peters, Weiqiang Xie, Lin Chang, Boqiang Shen, Heming Wang, Qi-Fan Yang, David Kinghorn, Mario Paniccia, Kerry J. Vahala, Paul A. Morton, and John E. Bowers, High-performance lasers for fully integrated silicon nitride photonics, *Nat. Commun.* **12**, 1 (2021).
- [40] Stijn Cuyvers, Bahawal Haq, Camiel Op de Beeck, Stijn Poelman, Artur Hermans, Zheng Wang, Agnieszka Gocalinska, Emanuele Pelucchi, Brian Corbett, Gunther Roelkens, Kasper Van Gasse, and Bart Kuyken, Low noise heterogeneous III-V-on-silicon-nitride mode-locked comb laser, *Laser Photonics Rev.* **15**, 2000485 (2021).
- [41] B. Dahmani, L. Hollberg, and R. Drullinger, Frequency stabilization of semiconductor lasers by resonant optical feedback, *Opt. Lett.* **12**, 876 (1987).
- [42] P. Laurent, A. Clairon, and C. Breant, Frequency noise analysis of optically self-locked diode lasers, *IEEE J. Quantum Electron.* **25**, 1131 (1989).
- [43] Anatolii N. Oraevsky, Alexander V. Yarovitsky, and Vladimir L. Velichansky, Frequency stabilisation of a diode laser by a whispering-gallery mode, *Quantum Elec. (Woodbury)* **31**, 897 (2001).
- [44] W. Liang, V. S. Ilchenko, A. A. Savchenkov, A. B. Matsko, D. Seidel, and L. Maleki, Whispering-gallery-mode-resonator-based ultranarrow linewidth external-cavity semiconductor laser, *Opt. Lett.* **35**, 2822 (2010).
- [45] W. Liang, D. Eliyahu, V. S. Ilchenko, A. A. Savchenkov, A. B. Matsko, D. Seidel, and L. Maleki, High spectral purity Kerr frequency comb radio frequency photonic oscillator, *Nat. Commun.* **6**, 7957 (2015).
- [46] W. Liang, V. S. Ilchenko, D. Eliyahu, A. A. Savchenkov, A. B. Matsko, D. Seidel, and L. Maleki, Ultralow noise miniature external cavity semiconductor laser, *Nat. Commun.* **6**, 7371 (2015).
- [47] N. M. Kondratiev, V. E. Lobanov, A. V. Cherenkov, A. S. Voloshin, N. G. Pavlov, S. Koptyaev, and M. L. Gorodetsky, Self-injection locking of a laser diode to a high- Q WGM microresonator, *Opt. Express* **25**, 28167 (2017).
- [48] Ramzil R. Galiev, Nikita M. Kondratiev, Valery E. Lobanov, Andrey B. Matsko, and Igor A. Bilenko, Optimization of Laser Stabilization via Self-Injection Locking to a Whispering-Gallery-Mode Microresonator, *Phys. Rev. Appl.* **14**, 014036 (2020).
- [49] Andrey S. Voloshin, Nikita M. Kondratiev, Grigory V. Lihachev, Junqiu Liu, Valery E. Lobanov, Nikita Yu. Dmitriev, Wenle Weng, Tobias J. Kippenberg, and Igor A. Bilenko, Dynamics of soliton self-injection locking in optical microresonators, *Nat. Commun.* **12**, 235 (2021).
- [50] Boqiang Shen, Lin Chang, Junqiu Liu, Heming Wang, Qi-Fan Yang, Chao Xiang, Rui Ning Wang, Jijun He, Tianyi Liu, Weiqiang Xie, Joel Guo, David Kinghorn, Lue Wu, Qing-Xin Ji, Tobias J. Kippenberg, Kerry Vahala, and John E. Bowers, Integrated turnkey soliton microcombs, *Nature* **582**, 365 (2020).
- [51] Arslan S. Raja, Andrey S. Voloshin, Hairun Guo, Sofya E. Agafonova, Junqiu Liu, Alexander S. Gorodnitskiy, Maxim Karpov, Nikolay G. Pavlov, Erwan Lucas, Ramzil R. Galiev, Artem E. Shitikov, John D. Jost, Michael L. Gorodetsky, and Tobias J. Kippenberg, Electrically pumped photonic integrated soliton microcomb, *Nat. Commun.* **10**, 680 (2019).
- [52] Brian Stern, Xingchen Ji, Yoshitomo Okawachi, Alexander L. Gaeta, and Michal Lipson, Battery-operated integrated frequency comb generator, *Nature* **562**, 401 (2018).
- [53] T. J. Kippenberg, R. Holzwarth, and S. A. Diddams, Microresonator-based optical frequency combs, *Science* **332**, 555 (2011).
- [54] Guoping Lin, Aurélien Coillet, and Yanne K. Chembo, Nonlinear photonics with high- Q whispering-gallery-mode resonators, *Adv. Opt. Photon.* **9**, 828 (2017).
- [55] Alessia Pasquazi, Marco Peccianti, Luca Razzari, David J. Moss, Stéphane Coen, Miro Erkintalo, Yanne K. Chembo, Tobias Hansson, Stefan Wabnitz, Pascal Del'Haye, Xiaoxiao Xue, Andrew M. Weiner, and Roberto Morandotti, Micro-combs: A novel generation of optical sources, *Phys. Rep.* **729**, 1 (2018).
- [56] Alexander L. Gaeta, Michal Lipson, and Tobias J. Kippenberg, Photonic-chip-based frequency combs, *Nat. Photonics* **13**, 158 (2019).
- [57] Andre Kovach, Dongyu Chen, Jinghan He, Hyungwoo Choi, Adil Han Dogan, Mohammadreza Ghasemkhani, Hossein Taheri, and Andrea M. Armani, Emerging material systems for integrated optical Kerr frequency combs, *Adv. Opt. Photonics* **12**, 135 (2020).
- [58] Tong Lin, Avik Dutt, Chaitanya Joshi, Xingchen Ji, Christopher T. Phare, Yoshitomo Okawachi, Alexander L. Gaeta, and Michal Lipson, Broadband ultrahigh-resolution chip-scale scanning soliton dual-comb spectroscopy, arXiv preprint [arXiv:2001.00869](https://arxiv.org/abs/2001.00869) (2020).
- [59] Chengying Bao, Myoung-Gyun Suh, and Kerry Vahala, Microresonator soliton dual-comb imaging, *Optica* **6**, 1110 (2019).

- [60] Avik Dutt, Chaitanya Joshi, Xingchen Ji, Jaime Cardenas, Yoshitomo Okawachi, Kevin Luke, Alexander L. Gaeta, and Michal Lipson, On-chip dual-comb source for spectroscopy, *Sci. Adv.* **4**, e1701858 (2018).
- [61] Weiqiang Wang, Wenfu Zhang, Zhizhou Lu, Sai T. Chu, Brent E. Little, Qinghua Yang, Lei Wang, and Wei Zhao, Self-locked orthogonal polarized dual comb in a microresonator, *Photonics Res.* **6**, 363 (2018).
- [62] Mengjie Yu, Yoshitomo Okawachi, Austin G. Griffith, Nathalie Picqué, Michal Lipson, and Alexander L. Gaeta, Silicon-chip-based mid-infrared dual-comb spectroscopy, *Nat. Commun.* **9**, 1 (2018).
- [63] N. G. Pavlov, G. Lihachev, S. Koptyaev, E. Lucas, M. Karpov, N. M. Kondratiev, I. A. Bilenko, T. J. Kippenberg, and M. L. Gorodetsky, Soliton dual frequency combs in crystalline microresonators, *Opt. Lett.* **42**, 514 (2017).
- [64] See Supplemental Material at <http://link.aps.org/supplemental/10.1103/PhysRevApplied.18.034068> for additional information about theoretical microcomb efficiency estimations, chip matching, and different laser diode comparison.
- [65] Xiaoxiao Xue, Yi Xuan, Cong Wang, Pei-Hsun Wang, Yang Liu, Ben Niu, Daniel E. Leaird, Minghao Qi, and Andrew M. Weiner, Thermal tuning of Kerr frequency combs in silicon nitride microring resonators, *Opt. Express* **24**, 687 (2016).
- [66] Junqiu Liu, Hao Tian, Erwan Lucas, Arslan S. Raja, Grigory Lihachev, Rui Ning Wang, Jijun He, Tianyi Liu, Miles H. Anderson, Wenle Weng, Sunil A. Bhave, and Tobias J. Kippenberg, Monolithic piezoelectric control of soliton microcombs, *Nature* **583**, 385 (2020).
- [67] Warren Jin, Qi-Fan Yang, Lin Chang, Boqiang Shen, Heming Wang, Mark A. Leal, Lue Wu, Maodong Gao, Avi Feshali, Mario Paniccia, Kerry J. Vahala, and John E. Bowers, Hertz-linewidth semiconductor lasers using CMOS-ready ultra-high- Q microresonators, *Nat. Photonics* **15**, 346 (2021).
- [68] T. Herr, V. Brasch, J. D. Jost, C. Y. Wang, N. M. Kondratiev, M. L. Gorodetsky, and T. J. Kippenberg, Temporal solitons in optical microresonators, *Nat. Photonics* **8**, 145 (2014).
- [69] H. Guo, M. Karpov, E. Lucas, A. Kordts, M. H. P. Pfeiffer, V. Brasch, G. Lihachev, V. E. Lobanov, M. L. Gorodetsky, and T. J. Kippenberg, Universal dynamics and deterministic switching of dissipative Kerr solitons in optical microresonators, *Nat. Phys.* **13**, 94 (2016).
- [70] T. Herr, V. Brasch, J. D. Jost, I. Mirgorodskiy, G. Lihachev, M. L. Gorodetsky, and T. J. Kippenberg, Mode Spectrum and Temporal Soliton Formation in Optical Microresonators, *Phys. Rev. Lett.* **113**, 123901 (2014).
- [71] Chanju Kim, Kresten Yvind, and Minhao Pu, Suppression of avoided resonance crossing in microresonators, *Opt. Lett.* **46**, 3508 (2021).
- [72] Qing Li, Travis C. Briles, Daron A. Westly, Tara E. Drake, Jordan R. Stone, B. Robert Ilic, Scott A. Diddams, Scott B. Papp, and Kartik Srinivasan, Stably accessing octave-spanning microresonator frequency combs in the soliton regime, *Optica* **4**, 193 (2017).
- [73] Chaitanya Joshi, Jae K. Jang, Kevin Luke, Xingchen Ji, Steven A. Miller, Alexander Klenner, Yoshitomo Okawachi, Michal Lipson, and Alexander L. Gaeta, Thermally controlled comb generation and soliton mode-locking in microresonators, *Opt. Lett.* **41**, 2565 (2016).
- [74] Naoya Kuse, Tomohiro Tetsumoto, Gabriele Navickaite, Michael Geiselmann, and Martin E. Fermann, Continuous scanning of a dissipative Kerr-microresonator soliton comb for broadband, high-resolution spectroscopy, *Opt. Lett.* **45**, 927 (2020).
- [75] Nikita M. Kondratiev, Ramzil R. Galiev, and Valery E. Lobanov, in *Nonlinear Optics and Applications XII*, Vol. 11770, edited by Mario Bertolotti, Anatoly V. Zayats, and Alexei M. Zheltikov, International Society for Optics and Photonics (SPIE, Czech Republic, 2021), p. 53.
- [76] Nikita M. Kondratiev, Valery E. Lobanov, Evgeny A. Lonshakov, Nikita Yu. Dmitriev, Andrey S. Voloshin, and Igor A. Bilenko, Numerical study of solitonic pulse generation in the self-injection locking regime at normal and anomalous group velocity dispersion, *Opt. Express* **28**, 38892 (2020).
- [77] Nikita M. Kondratiev and Valery E. Lobanov, Modulational instability and frequency combs in whispering-gallery-mode microresonators with backscattering, *Phys. Rev. A* **101**, 013816 (2020).
- [78] Cyril Godey, Irina V. Balakireva, Aurélien Coillet, and Yanne K. Chembo, Stability analysis of the spatiotemporal Lugiato-Lefever model for Kerr optical frequency combs in the anomalous and normal dispersion regimes, *Phys. Rev. A* **89**, 063814 (2014).
- [79] Xiaoxiao Xue, Pei-Hsun Wang, Yi Xuan, Minghao Qi, and Andrew M. Weiner, Microresonator Kerr frequency combs with high conversion efficiency, *Laser Photonics Rev.* **11**, 1600276 (2017).
- [80] Bok Young Kim, Yoshitomo Okawachi, Jae K. Jang, Mengjie Yu, Xingchen Ji, Yun Zhao, Chaitanya Joshi, Michal Lipson, and Alexander L. Gaeta, Turn-key, high-efficiency Kerr comb source, *Opt. Lett.* **44**, 4475 (2019).
- [81] Jae K. Jang, Yoshitomo Okawachi, Yun Zhao, Xingchen Ji, Chaitanya Joshi, Michal Lipson, and Alexander L. Gaeta, Conversion efficiency of soliton Kerr combs, *Opt. Lett.* **46**, 3657 (2021).
- [82] Changjing Bao, Lin Zhang, Andrey Matsko, Yan Yan, Zhe Zhao, Guodong Xie, Anuradha M. Agarwal, Lionel C. Kimerling, Jurgen Michel, Lute Maleki, and Alan E. Willner, Nonlinear conversion efficiency in Kerr frequency comb generation, *Opt. Lett.* **39**, 6126 (2014).
- [83] Maxim Karpov, Martin H. P. Pfeiffer, Hairun Guo, Wenle Weng, Junqiu Liu, and Tobias J. Kippenberg, Dynamics of soliton crystals in optical microresonators, *Nat. Phys.* **15**, 1071 (2019).
- [84] Qi-Fan Yang, Xu Yi, Ki Youl Yang, and Kerry Vahala, Counter-propagating solitons in microresonators, *Nat. Photonics* **11**, 560 (2017).
- [85] Dmitry A. Chermoshentsev, Artem E. Shitikov, Evgeny A. Lonshakov, Georgy V. Grechko, Ekaterina A. Sazhina, Nikita M. Kondratiev, Anatoly V. Masalov, Igor A. Bilenko, Alexander I. Lvovsky, and Alexander E. Ulanov, Dual-laser self-injection locking to an integrated microresonator, *Opt. Express* **30**, 17094 (2022).
- [86] M. L. Gorodetsky, A. D. Pryamikov, and V. S. Ilchenko, Rayleigh scattering in high- Q microspheres, *J. Opt. Soc. Am. B* **17**, 1051 (2000).